JOURNAL OF SPACECRAFT AND ROCKETS
Vol. 39, No. 3, May–June 2002

Plasma Response to Jump of Insulator Surface Potential in Ionospheric Plasma Environment

Mengu Cho,* Raju Ramasamy,† and Masayuki Hikita‡
Kyushu Institute of Technology, Kitakyushu 804, Japan
and
Koji Tanaka§ and Susumu Sasaki¶
Institute of Space and Astronautical Sciences, Kanagawa 229, Japan

Once an arc occurs on a solar array in low Earth orbit, it might grow by taking charges from a remotely located insulator through a current path formed by the plasma. A laboratory experiment and a computer simulation are carried out to study the response of plasma to a sudden potential change of the insulator surface induced by arcing on a solar array in low-Earth-orbit plasma environment. The experiment gives an artificial potential jump to the insulator surface. The simulation employs a Monte Carlo particle-in-cell method in axisymmetrical two-dimensional space that simulates the laboratory experiment. When a set of simulation parameters as close as possible to the experiment is used, the unsteady response of the plasma observed in the experiment is reproduced very well. Once the insulator surface potential jumps up due to arcing, a positive sheath develops. If the neutral density is high enough to be of the order of magnitude of 10^{18} m^{-3}, explosive expansion of the sheath is set off due to the feedback mechanism induced by ionization inside the sheath. The explosive sheath expansion alone, however, cannot explain the current path formation between the array and the insulator observed in the arcing experiment, and the importance of electrons ejected from the arc spot on the onset of arcing is pointed out.

Nomenclature

B_z = axial magnetic field, G
I_p = peak of discharge current, A
m = particle mass, kg
n = number density, m^{-3}
r = radial position, cm
T_e = electron temperature, eV
t = time, s
V = potential, V
V_b = array bias voltage, V
V_{pr} = probe signal, V
V_s = step-bias voltage, V
z = axial position, cm
z_p = probe axial axial position, cm
Δr = grid size in radial direction, m
Δt = time step, s
Δz = grid size in axial direction, m

Subscripts

e = electron
i = ion
n = neutral

I. Introduction

WHEN a spacecraft has a high voltage within its body and the high-voltage surface is exposed, most of the high voltage becomes negative with respect to the electric potential of the surrounding plasma. If the spacecraft structural body is connected to the negative end of solar array, the spacecraft structure has a highly negative potential. The spacecraft body attracts positive ions from the surrounding plasma, and ions impact the body surface and solar array. The insulator on the spacecraft, such as solar array coverglass or thermal coatings, is charged and acts as a capacitance that stores the positive charge on the surface facing the plasma. If a conductor with a negative potential of the order of magnitude of 100 V is exposed to the plasma along with dielectric material, an arc occurs due to field intensification at the triple junction formed by conductor, dielectric, and plasma, such as an interconnector on a solar array.[1] Once an arc occurs on the spacecraft surface, the charge stored on the spacecraft insulator is supplied as the arc current. How much the arcing affects the spacecraft system depends on how much current and energy the arcing current carries into the spacecraft circuit.

In Ref. 2, a pair of one solar array and an electrode wrapped by an insulator film separated by 40 cm or longer was biased to a negative potential of −500 V or higher in a plasma chamber. Once an arc occurred on the solar array surface, the mirror image current of the arc current flew from the insulator electrode, which indicated that the charge on the insulator was supplied as the arc current. It was explained that a current path was formed in the plasma between the arc point on a array and the remotely located insulator because the current loop had to be closed. Once an arc occurred, electrons were ejected from the array to the surrounding plasma producing an electron-rich negative sheath, whose formation was inferred from the transient signal of a langmuir probe. At the same time, the potentials of the array and the electrode under the insulator jumped from the highly negative value to near zero. Then a positive sheath was formed near the insulator surface whose formation was also inferred from the transient signal of the langmuir probe. When the langmuir probe was moved inside the chamber, it was found that the plasma potential was more negative near the array and more positive near the insulator, which suggests that the negative sheath originated from the array and the positive sheath originated from the insulator. When the distance between the array and the insulator was short, the arc current had a long duration and dual peaks suggesting that the current path was formed in the plasma and the insulator charge was released. Also, the shorter the distance was, the more charge was flown as the arc current.

Presented as Paper 2001-0955 at the AIAA 39th Aerospace Sciences Meeting, Reno, NV, 8–11 January 2001; received 22 March 2001; revision received 24 August 2001; accepted for publication 30 August 2001.

*Associate Professor, Department of Electrical Engineering, Tobata-ku; cho@ele.kyutech.ac.jp. Member AIAA.
†Postdoctoral Fellow, Satellite Venture Business Laboratory, Tobata-ku.
‡Professor, Department of Electrical Engineering, Tobata-ku.
§Research Associate, Space Energy Division, Sagamihara.
¶Professor, Space Energy Division, Sagamihara.

The key mechanism of the current path formation is whether the positive sheath and the negative sheath can meet. The purpose of the present paper is to investigate the expansion mechanism of the positive sheath. This paper is a part of basic study on the current path formation, and we treat only the positive sheath. By studying the contribution from the positive sheath and the contribution from the negative sheath separately, we can reveal basic physical processes underlying the complex phenomena and can identify the synergetic effects produced by the two processes.

Once an arc occurs, the potential of the solar array increases rapidly from the negative bias voltage V_b to near zero, as shown in Figs. 5 and 6 of Ref. 2. For the case of real spacecraft, this increase corresponds to the situation where the spacecraft potential increases due to the sudden influx of positive charges into a spacecraft that can be regarded as one object floating in the plasma. The potential of the capacitance surface also increases suddenly from the near zero value to a positive value comparable to $|V_b|$ as the potential of underlying electrode increases.[3,4] In the present paper we carry out a controlled experiment by giving a potential jump to the electrode underlying the thin insulator, similar to the potential profile measured in the experiment of Ref. 2. We measure the plasma response to the potential jump by measuring the transient signal via a langmuir probe.

Another reason for carrying out the controlled experiment by biasing only a capacitance is that the situation becomes simple enough to carry out computer simulation matching most of the parameters to the experiment. By the use of computer simulation via a Monte Carlo particle-in-cell code, we can visualize the phenomena occurring in the experimental condition, especially how the surrounding plasma is responding to the sudden change of the insulator surface potential. Doing so via experimental alone is difficult because the measurement by a probe gives data only on discrete points. We also change the neutral density and magnetic field, which is usually difficult to change in the experiment, to see their effects on the sheath formation.

In the second part of this paper, we describe the experiment and its results. In the third part, we describe the computational code and the results. We verify the code by comparing the probe signals measured in the experiment and calculated by the simulation. Once we have agreement in a macroscopic value, we can use the computer simulation as a tool to investigate microscopic phenomena. Also, we study the effects of neutral density and magnetic field by varying the simulation parameters. In the fourth part, we discuss the necessary conditions of the current path formation based on the finding made by the simulation. Finally, in the fifth part, we conclude the paper and suggest future work.

II. Experiment

A. Experimental Setup

In Fig. 1, the experimental setup for the experiment is shown, which is very similar to the one shown in Fig. 4 of Ref. 2. Actually we did the experiment on the same week with the same facility as Ref. 2 without breaking the vacuum. The chamber plasma is produced by a backdiffusion-type argon plasma source with an exit diameter of 20 cm. In the plasma source, a dc bias of approximately 200 V is applied between the grounded cathode and the anode, where the cathode is made of hot tungsten wire and electrons are emitted by thermal emission. This bias voltage of 200 V should be kept in mind when we compare the simulation results to the experimental results in Sec. III.A. The plasma condition, gas pressure, the magnetic field, and the lagmuir probes were the same as those of Ref. 2. The only differences were that we biased only the capacitance 2 and that a stepwise voltage was given by a thyristor switch. The four-channel oscilloscope measured the electrode potential, the current flowing to the capacitance 2 via a current probe, and the moving probe via a voltage probe across a 100-kΩ resistance. The oscilloscope was triggered when the electrode potential rose across 52 V and the sampling rate was 50 MS/s.

The coordinate system of the probe position was the same as that of Ref. 2. Capacitance 2 was located at $y = 40$ cm and $z = 0$. The thyristor switch could provide a step bias from 5 to the 95% of the peak value in 0.5 μs and supply a step voltage as high as 2500 V. The

Table 1 Parameters of experiment

Case	Bias voltage V_s, V	Probe position, cm
E1	434	$z = 5$–100, $y = -50$–70
E2	175 ~ 690	$z = 50$, $y = 40$
E3	85 ~ 690	$z = 10$, $y = 40$

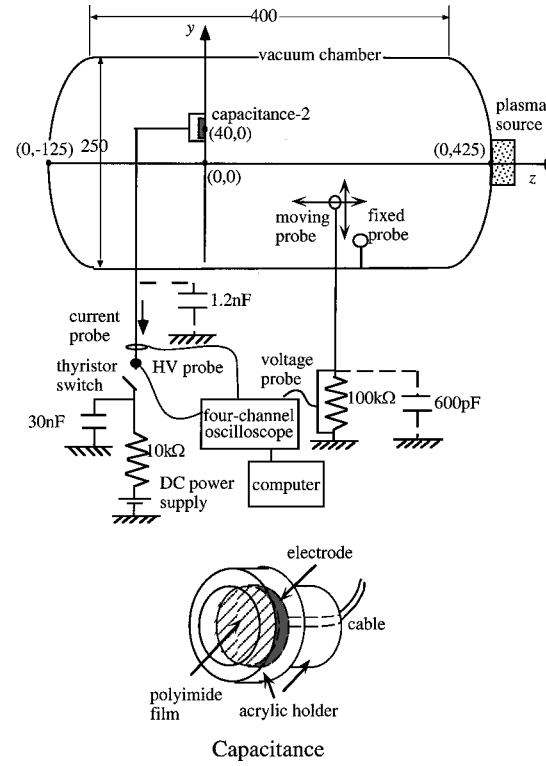

Fig. 1 Experimental setup of step-bias experiment.

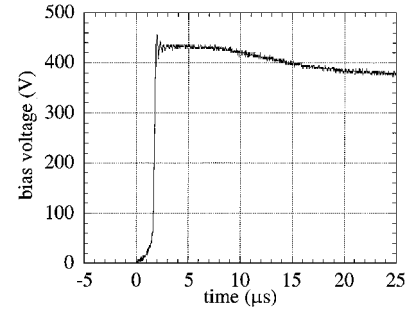

Fig. 2 Example of temporal profile of bias voltage applied to the electrode.

30-nF capacitance connected to the external circuit prevented the step bias from decaying after the switch was turned on. During the experiment, each step bias was applied with an interval of 10 s or longer. We carried out three cases for the experiment, which are listed in Table 1.

The probe signal was also very susceptible to external high-frequency noise (2 MHz or higher). To minimize the effect of noise, we carried out a Fourier transform of all of the waveforms, including the currents and the voltage, and filtered out frequencies higher than 2 MHz. This filtering limited the time resolution of the experiment to 0.5 μs. The resistance of 100 kΩ connected to the probe was chosen so that the small amount of current, such as an ion saturation current in the density measurement, can be measured as the voltage across the resistance. At the same time, however, the cable connecting the probe has a capacitance of 600 pF to the ground and the current with the timescale faster than 100 kΩ × 600 pF = 60 μs cannot be measured directly. Then the probe acts as an ac potential probe (it cannot measure the dc potential) with the bandwidth between 16.6 kHz and 2 MHz.

In Fig. 2, a typical waveform of the electrode potential is shown. The original waveform recorded by the oscilloscope has the time zero when the oscilloscope was triggered at the threshold of 52 V. The waveform has been shifted by 1.6 μs to the right so that the beginning of the step pulse coincides with the time zero. This shift is necessary to match the time between the experiment and the simulation. This waveform is also used as the temporal profile of the electrode potential in the simulation cases S1–S4 and S8–S14. The potential gives a small overshoot once it reaches the peak value as shown at $t \simeq 2$ μs in Fig. 2. The step-bias voltage is defined as the time-averaged potential from 2.6 to 4.6 μs after this overshoot decays.

The waveform shown in Fig. 2 is similar to the waveform of array potential observed in two-peak-type discharge in Ref. 2, though the time is shifted and it starts from 0 instead of $V_b(<0)$. The current waveform of a two-peak-type discharge has the second peak while the array potential is still near zero (see Fig. 6 of Ref. 2). Therefore, when the steady electrode potential is kept at least for that duration, 10–15 μs from the beginning of the step bias, the step bias can simulate the potential profile of the arc experiment. The rise time, however, is a little too fast for the step bias by about 1.5 μs compared to the potential rise in the arc experiment. Therefore, the positive sheath expansion in the step-bias experiment would be accelerated a little compared to the arc experiment.

B. Experimental Result

In Fig. 3, typical waveforms obtained in the experiment are shown. The waveforms are taken from a result of case E1, where the capacitance 2 is step biased to +434 V and the probe position is $z = 10$ cm and $y = 40$ cm. The high-frequency oscillation near time zero is noises due to the switching of the thyristor. The waveforms has been shifted by 1.6 μs to the right from the originals recorded by the oscilloscope. We have a positive peak, V_{pr4}, at T_{pr4}, several microseconds after the bias is applied. Unlike the waveforms of the arc experiment shown in Figs. 5 and 6 of Ref. 2, the probe signal in Fig. 3 does not show the initial negative peak because no arc occurs for this case and no negative sheath is formed. The probe transient after 4 μs, however, is very similar to the one-peak-type discharge (see Figs. 5 and 8 of Ref. 2) and to the two peak near the capacitance (see $y = 40$ cm of Fig. 11 of Ref. 2).

In Fig. 4, the peak values V_{pr4} measured in the case E1 are plotted. For the case of the step-bias experiment, the electrode potential jumped by 434 V from 0 to 434 V within 2 μs, as shown in Fig. 2. The probe position was changed along the y axis keeping the axial position at $z = 10$ cm. The peak value increases sharply when the probe is located in front of capacitance 2. A similar plot is found in Fig. 10 of Ref. 2, where the probe signals V_{pr3} for the one-peak-type discharge and V_{pr2} for the two-peak-type discharge are plotted. The peak values also increase when the probe is placed near capacitance 2. The similarity of the probe signal measured in the present experiment with the signals measured in the previous arc experiment supports the idea that the positive sheath develops due to the sudden jump of the insulator surface potential.

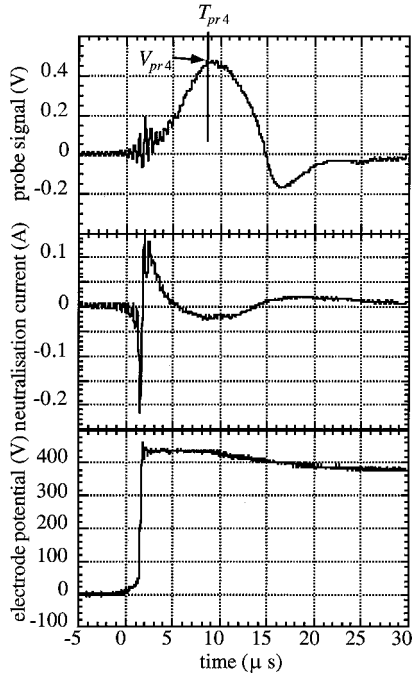

Fig. 3 Examples of typical waveforms observed in the step-bias experiment.

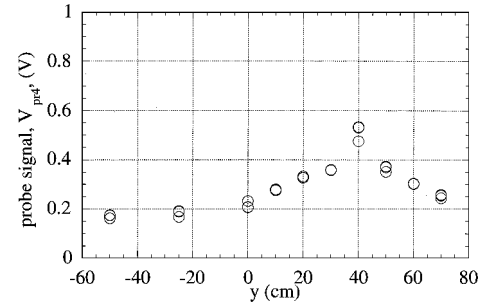

Fig. 4 Probe peak signals for the step-bias experiment, V_{pr4}, measured at different positions along y axis in case E1.

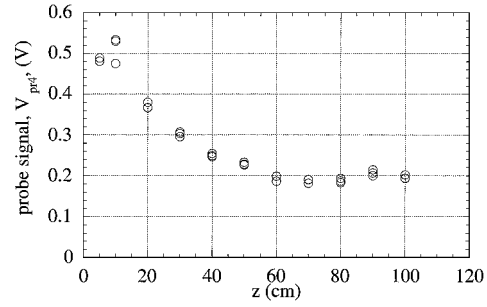

Fig. 5 Probe peak signals for the step-bias experiment, V_{pr4}, measured at different positions along z axis in case E1.

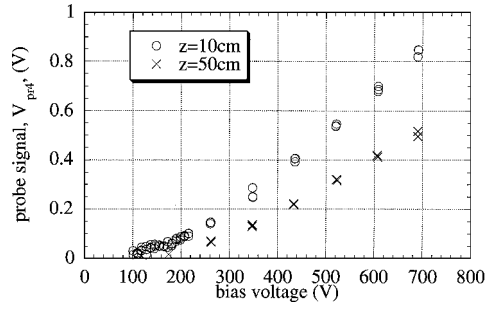

Fig. 6 Probe peak signals for the step-bias experiment, V_{pr4}, measured for different step-bias voltages in cases E2 and E3.

The characteristics shown in Fig. 4 also shows that the positive sheath has its center at the insulator surface. To support this idea, in Fig. 5 we plot the peak values V_{pr4}, measured at different locations along z axis, the direction perpendicular to the surface, while fixing the y position at $y = 40$ cm. In Fig. 5, the results of case E1 are plotted. The peak value decreases as the distance between the probe and the insulator surface increases. It also shows saturation at the distance of 60 cm or longer.

If the peak of probe signal V_{pr4} is due to the jump of the insulator surface potential, the larger the potential jump is, the larger and the faster it should appear. Figures 6 and 7, show the peak value V_{pr4} and its time T_{pr4} measured at $y = 40$ cm and $z = 10$ cm and $y = 40$ cm and $z = 50$ cm for different bias voltages in the cases E2 and E3. As the step-bias voltage increases, the peak value increases, and the peak time decreases, again supporting the idea of positive sheath formation. Figure 7 also shows that the peak time T_{pr4} does not depend on the probe axial location for the same step-bias voltage. Whereas the peak amplitude depends on the probe position, the peak time does not. We discuss the reason why via the computer simulation.

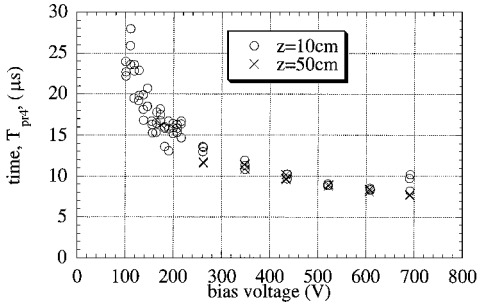

Fig. 7 Time of the probe peak signals for the step-bias experiment, T_{pr4}, measured for different step-bias voltages.

III. Simulation

A. Simulation Code

As the simulation scheme, we use the Monte Carlo particle-in-cell (PTC) method[5,6] that follows the motion of charged particles self-consistently with their own space charge and collisions with neutral particles. The simulation domain is axisymmetric, and we consider spatial variations only in the r and z directions, while all of the three components of particle velocities are considered. Figure 8 shows the computational domain. The computational domain simulates a slice of cylinder with an angle of 7×10^{-8} rad whose radius is 1.24 m and length is 3.3 m.

Initially, a plasma of uniform density ($n_e = n_i = 5 \times 10^{11}$ m^{-3}) with the Maxwellian distribution at $\kappa T_e = \kappa T_i = 2.4$ eV is loaded inside the computational domain, and once the simulation starts, no particle is added from the boundary. The plasma source is not included in the simulation. The plasma parameters simulate the experimental condition in Ref. 2. In a PIC code, a particle followed in the simulation represents a group of real charged particles or a fraction of a real particle, which is often called a superparticle. Each superparticle has its weight as an indicator of how many real particles it represents. If we load the superparticles with equal weighting, only few particles are loaded near the axis because the cell volume becomes increasingly small as the radius approaches zero.

To avoid this problem, we assign smaller weight to particles loaded near the axis, and load the superparticles so that an equal number of superparticles, 18, is loaded in each cell. Then the initial number of particles in the domain is 730,000 for each species. The ion to electron mass ratio is set to 73,400 to simulate the real mass ratio of an argon ion to an electron. The computational boundary is a fixed wall except for the center axis, to simulate the chamber wall, where the potential is set to zero. Once a particle reaches the wall, it is removed from the domain. The simulation time step is $\Delta t = 7.5 \times 10^{-10}$ s, and the simulation is run typically up to 15–32 μs. Typical computational time for one case is 2–4 days on a UNIX workstation with an Alpha 21264 500-MHz CPU.

The computational domain is filled with argon gas of uniform density n_n. Collision between charged particles and neutral argon is taken into account, though no motion of neutral argon is taken into account. Quantitative accuracy of the collision cross section was already checked against the the transport coefficient data, such as ionization and drift velocity, taken from the literature (see Ref. 6 for details). Once ionization collision occurs, a pair of secondary electrons and ions is placed with an appropriate energy at the collision point.

To simulate the insulator and electrode used in the experiment, we place an electrode insulated by acrylic and polyimide. The cylindrical coordinate of the computational domain has its center at the polyimide surface for comparison with the experiment. In the experiment, the insulator surface was 40 cm off axis from the chamber axis in the r direction. The effect caused by this slight difference is insignificant as long as the the sheath from the insulator does not extend over 85 cm, where the closest chamber wall existed in the experiment. The geometry reproduces the real geometry with the same thickness of the electrode, the polyimide, and the acrylic. The area of the polyimide film is also the same so that it has the same capacitance as the experiment. The dielectric constants are 3.5 for the polyimide and 2.7 for the acrylic. To model the thin film

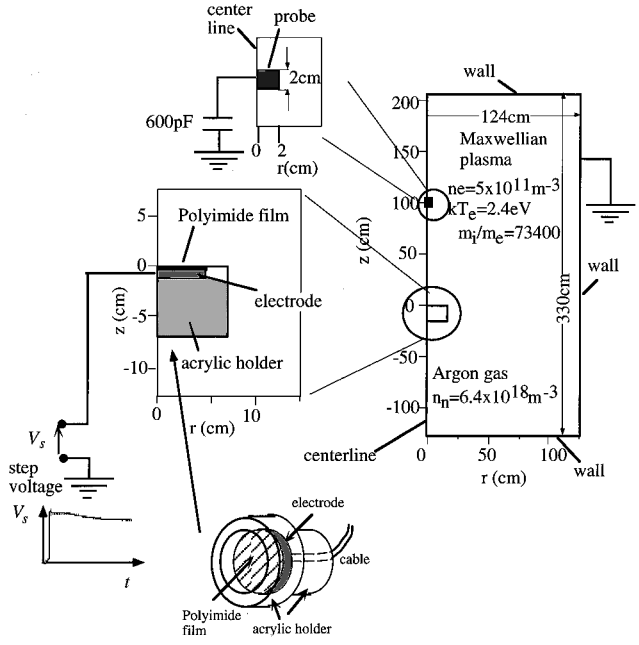

Fig. 8 Schematic of computational domain.

(7.5 μm), the computational grids are clustered in z directions using Eq. (5.220) of Ref. 7. The smallest grid size is $\Delta z = 2$ μm and the largest grid size is $\Delta z = 3$ cm. In the r direction, the grid size is equal to $\Delta r = 0.02$ m. The total number of grid points is 63 in the r direction and 651 in the z direction. Initially, the insulator surface, polyimide and acrylic, has a potential of zero. The initial surface charge to have the zero potential is calculated from the capacitance matrix method.[8] We give the same potential profile to the electrode as the experiment, such as the one shown in Fig. 2. The potential data are taken from the step-bias experiment and used as an input file for the potential profile in the simulation. Because in the experiment the oscilloscope was triggered at the threshold of 52 V and recorded that time as time zero, we have shifted the oscilloscope data by 1.6 μs as shown in Fig. 2 so that time zero corresponds to the time when the step pulse begins. The time 1.6 μs was chosen because the potential never went to negative after that time until the end of the record.

To validate the simulation code, we place a langmuir probe shaped like a fat disk, whose radius is 2 cm and the thickness is 2 cm. The planar surface is perpendicular to the z axis. In the experiment, the probe is a disk of 3 mm radius. The thickness is about 1 mm. The planar probe surface is parallel to the z axis in the experiment.

The probe current consists of displacement current and the conduction current. The displacement current is due to the time variation of the surface charge induced on the probe surface as the electric field on the surface varies. The conduction current is mainly due to ions entering the probe surface for the present case because the plasma potential is mostly positive with respect to the probe. As it was explained in Ref. 2, the probe signal in the experiment corresponds to the the time integral of the current because of the large resistance, 100 kΩ, compared to the parallel capacitance. Therefore, as a comparison, we calculate the surface charge induced on the probe surface by integrating the electric field perpendicular to the probe surface. By dividing the surface charge by the probe capacitance with respect to the ground, 600 pF, we can obtain the probe signal in the voltage as if it were observed in the experiment. Unfortunately, however, the probe signal calculated this way cannot be compared quantitatively because the electric field and the surface charge on the probe surface depend on the size and shape of the probe. Nevertheless, the probe signal in the experiment shows very similar temporal profile to the computationally calculated probe signal. In the simulation, the probe potential is fixed to zero, though the probe actually has a small potential equal to the probe signal output voltage, less than 1 V. Because the probe is surrounded by the plasma, whose space potential is 20 V or higher, this assumption on the probe potential causes no significant error.

Table 2 Parameters of Monte Carlo PIC simulation

Case	n_n, m^{-3}	z_p, cm	V_s, V	B_z, G
S1	6.5×10^{18}	10	434	0
S2	6.5×10^{18}	30	434	0
S3	6.5×10^{18}	50	434	0
S4	6.5×10^{18}	100	434	0
S5	6.5×10^{18}	10	174	0
S6	6.5×10^{18}	10	262	0
S7	6.5×10^{18}	10	690	0
S8	1.0×10^{16}	175	434	0
S9	1.0×10^{17}	175	434	0
S10	1.0×10^{18}	175	434	0
S11	2.0×10^{18}	175	434	0
S12	4.0×10^{18}	175	434	0
S13	6.5×10^{18}	175	434	0
S14	6.5×10^{18}	50	434	0.35

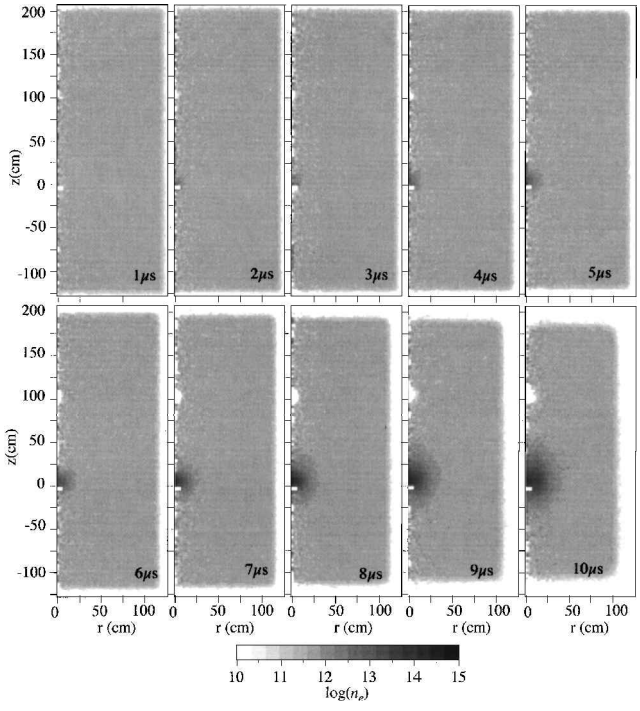

Fig. 9 Time variation of electron density (in m^{-3}) distribution calculated by the computer simulation for case S4.

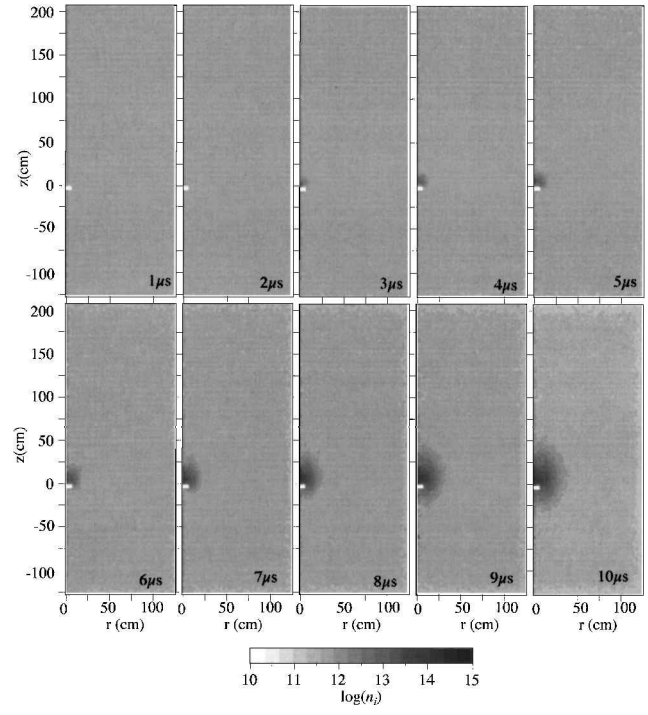

Fig. 10 Time variation of ion density (in m^{-3}) distribution calculated by the computer simulation for case S4.

In Table 2, we list the parameters used in each case of simulation. Cases S1–S4 are to check the simulation results against the experimental results comparing the probe signals. Cases S5–S7 are to investigate the effects of step-bias voltage and compare the results against the experimental results. Cases S8–S13 are to investigate the effects of neutral density on the sheath expansion. To avoid the effects of probe presence, the probe was placed far away from the insulator. Case S14 is to investigate the effect of magnetic field. The experiment in Ref. 2 was carried out by canceling the geomagnetic field to less than 0.09 G to make the analysis easier. The chamber axis (z axis) was at the north–south direction at the latitude of 36° and the eastern longitude of 140°. To investigate the effect of magnetic field, we apply $B = 0.35$ G along the z axis.

B. Simulation Result

In Figs. 9 and 10, the temporal profile of the electron and ion density are shown, respectively, for case S4. The densities are in m^{-3}. In Figs. 9 and 10, the insulator surface is at $z = 0$ and $r = 0$. The probe, whose potential is fixed to zero, is located at $z = 100$ cm and $r = 0$. Initially, the plasma potential inside the chamber is zero everywhere. Once the simulation is started, electrons near the chamber wall are rapidly absorbed, and a thin sheath appears near the chamber wall. The potential of the whole plasma increases due to the loss of negative charge. This phenomenon occurs to any plasma produced inside a finite volume, where the plasma has a positive potential with respect to the wall. When no bias is applied, the plasma potential becomes nearly steady at approximately 20 V in 10 μs. Once the bias is applied to the electrode and the insulator surface potential jumps up, electrons near the insulator are absorbed by the insulator surface. Then a small positive sheath appears near the insulator (see 2 μs in Figs. 9 and 10). At $t \simeq 3$ μs, concentration of ions begins to build up near the insulator surface, and the sheath keeps growing.

These ions are produced due to ionization of neutral argon. Although the ionization mean free path is about 10 m at its shortest for this neutral density, the small amount of ionization still occurs via electrons coming to the insulator surface. In the laboratory experiment, we observed by naked eye a flash of light near the insulator surface when the step bias of 690 V is applied. Ions move much slower than electrons, and they stay for a long time near the insulator. The secondary electrons produced by ionization are quickly absorbed by the insulator. Then the charge balance inside the sheath is tilted. The sheath boundary is determined so that the space charge inside the sheath makes the electric field at the boundary zero. To compensate the increase of the positive charge, the sheath must collect more negative charge, that is, electrons, by extending the sheath boundary farther outward. Additional electrons are collected by the sheath. However, because they run for a longer distance inside the sheath, there is a greater chance of making an ionization collision. Therefore, there is a feedback mechanism that further expands the sheath outward, which is the so-called sheath explosion studied in Refs. 9–11. As electrons are drawn to the insulator, a void of electrons is formed near the chamber wall. The total charge inside the chamber becomes more and more positive. As a result, a whole plasma potential inside the chamber increases. Figure 11 shows the potential distribution at $t = 9$ μs inside the chamber. The plasma potential is elevated to as high as 130 V, but it is rather uniform except near the insulator where the sheath is formed.

Figure 12 shows the temporal profile of the electric potential calculated in case S4. The probe is placed at $r = 0$ and $z = 100$ cm, and we see a spot of zero potential. In Fig. 12, we plot the equipotential contours at every 100 V for $t > 7$ μs. We see that the chamber plasma potential increases sharply between $t = 8$ and 9 μs. This time corresponds to the peak time T_{pr4} observed in the step bias experiment in Ref. 2.

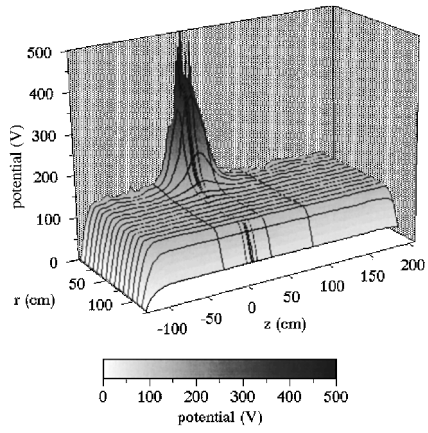

Fig. 11 Potential distribution at $t = 9$ μs calculated for case S4.

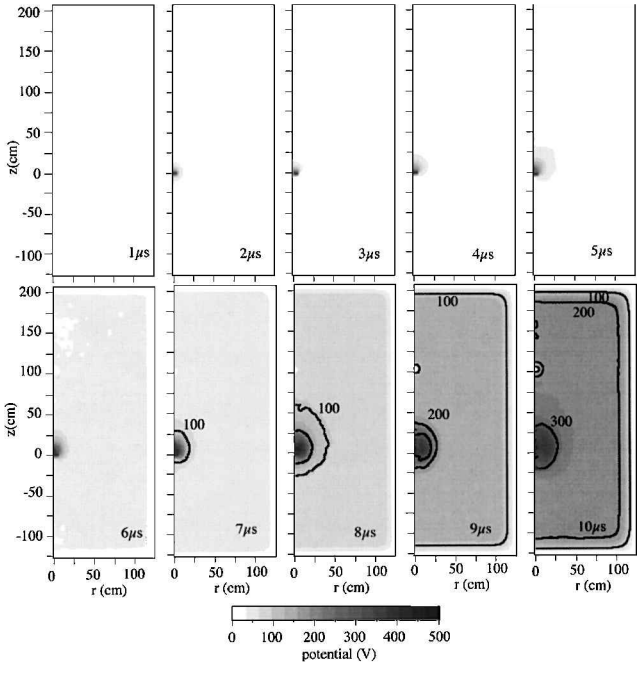

Fig. 12 Time variation of electric potential calculated by the computer simulation for case S4.

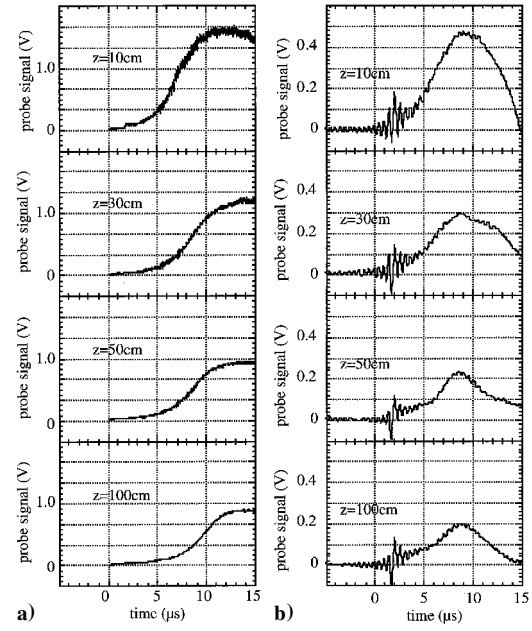

Fig. 13 Comparison of probe signals between a) simulation and b) experiment.

In the experiment, the chamber plasma is produced by a backdiffusion-type argon plasma source. In the plasma source, a dc bias of approximately 200 V is applied between the grounded cathode and the anode. It is essentially a dc glow discharge, and the plasma density inside the plasma source is estimated to be of the order of magnitude of 10^{14} m^{-3} with a temperature of a few electron volts. At a normal condition, the plasma source emits a plasma flow via ambipolar diffusion of ions and electrons. The plasma potential inside the plasma source is generally higher than the chamber plasma potential so that the plasma is extracted and compensates the loss of charged particles to the chamber wall. When the plasma density of $n_e = 5 \times 10^{11}$ m^{-3}, the temperature of $\kappa T_e = 2.4$ eV, and the chamber area of 40 m^2 are considered, the thermal flux of ions lost to the wall at the normal condition is approximately 10 mA, translated into the current, which is compensated by the plasma source via ambipolar diffusion.

For the present case, however, the chamber plasma potential changes rapidly after the switch on of the thyristor. As the chamber plasma potential becomes higher than the plasma potential inside the plasma source, for example, 8–9 μs, the plasma source no longer acts as a plasma source. It becomes an electron source. The thermal flux of electrons is far greater than the ambipolar diffusion flux. Therefore, once the plasma source becomes an electron source, it can quickly supply enough electrons to lower the elevated plasma potential inside the chamber.

Figure 13 shows the signal calculated for cases S1–S4 at different probe positions along z axis. The probe positions are $r = 0$ and are varied in z. The probe signal in volts that is shown is calculated by dividing the surface charge on the probe by the capacitance, 600 pF. In Fig. 13, the probe signals measured in experiment case E1 are also plotted. The high-frequency oscillation at $t \simeq 2$ μs of the experiment is noise due to switching of the thyristor. The probe signals of the simulation and the experiment cannot be compared quantitatively by plotting with the same vertical axis because the sizes of the probe are different, causing the shape of the sheath surrounding the probe to be different. Nevertheless, the probe signal of the simulation shows the rate of increase very similar to the experimental rate before $t =$ 8–9 μs. In the simulation, the probe signal reaches a steady value because there are no electrons from the plasma source to lower the elevated plasma potential. The rate of increase changes at $t =$ 6–7 μs, and the simulation even reproduces this change. The relative intensities among the different probe locations also agree between the simulation and the experiment.

The probe signals in the experiment have peaks at $t = 8$–10 μs irrespective of the probe position because the chamber potential increases are so high, over 100 V, that the plasma source emits electrons lowering the chamber potential rapidly. This explanation fits Fig. 7, where the peak time T_{pr4} does not differ much between the probe positions. Because the whole plasma potential is lowered, the probe peak appears almost simultaneously at every point inside the chamber. In the present simulation, we do not include the plasma source. Therefore, once the chamber plasma potential becomes near 100 V, it is no longer correct. However before that, $t \leq 8$–9 μs, while the plasma source is acting as a plasma source, we can neglect its presence because the amount of current, 10 mA, provided by the plasma source is negligible compared to the electron charge drawn to the insulator. When the potential disturbance is given by a step bias to the electrode, the amount of electrons drawn to the insulator is of the order of magnitude of 10^{-6} C. Therefore, even if we include the plasma flow of 10 mA from the outside in the simulation, it has little effect on the results in the timescale of the simulation time, 10–20 μs.

Figure 14 shows the temporal variation of potential at $r = 0$ and $z = 175$ cm calculated for cases S1 and S5–S7 changing the step-bias voltages. We use the potential at this location as an indicator to know when the chamber potential jumps over 100 V. The higher the bias voltage is, the faster the chamber potential increases. We do not know the exact potential where plasma source acts as the electron source giving the peak to the probe signal, though it is between several tens of volts and 200 V. If we set the threshold arbitrarily to 100 V for the moment, the chamber potential reaches that value

at $t = 6$, 8, 11, and 14 μs for the case of $V_s = 690$, 434, 262, and 174 V, respectively. These numbers agree with the T_{pr4} measured in the experiment and plotted in Fig. 7 within 2 μs for each bias voltage.

Figure 15 shows the temporal profile of the spatial distribution of the electric field amplitude calculated in case S4. Figure 15 was created to visualize the sheath boundary that is not always clear in the plot of density or potential. The sheath boundary is clearly seen around the insulator ($z = 0$ and $r = 0$), where the field amplitude becomes as strong as 1000 V/m or more. The sheath also grows into the $-z$ direction as the field line from the electrode penetrates the acrylic holder. The sheath expansion is fastest in the forward direction, that is, the $+z$ direction, which is best seen at time 7 μs. This observation supports the explanation made for the experimental results that the two-peak-type discharge occurred faster for the case where the insulator and the solar array were placed face-to-face than in the case where the insulator and the solar array were placed side-by-side (see Fig. 10 of Ref. 2).

Figure 16 shows the potential distribution near the insulator surface at $t = 10$ and 20 μs for various neutral densities. Figure 16 shows the simulation results of cases S8–S13. The equipotential contour lines are at every 50 V. For the neutral density $n_n \geq 4.0 \times 10^{18}$ m^{-3}, we see the plasma potential outside the sheath is already higher than 100 V at $t = 10$ μs. Also, the higher the neutral density is, the larger the sheath size becomes. For the neutral density of 2.0×10^{18} m^{-3}, we still see the contour line of 50 V that is extending outward at $t = 10$ μs. The chamber plasma potential eventually reaches 100 V at $t = 20$ μs, and we see that the sheath size becomes 50 cm in the z direction, 30 cm in the r direction, and 10 cm in the $-z$ direction, and keeps growing further. For the case with $n_n = 1.0 \times 10^{18}$ m^{-3}, the sheath never grows to such an extent and reaches steady state, though it is still larger than the lower density case, $n_n = 1.0 \times 10^{17}$ m^{-3}. There is no significant difference between the cases with $n_n = 1.0 \times 10^{17}$ and 1.0×10^{16} m^{-3}. Therefore, we can conclude that for this set of parameters the threshold over which the explosive sheath expansion occurs is somewhere between $n_n = 1.0 \times 10^{18}$ and 2.0×10^{18} m^{-3}. Although, this density sounds very high as a density at the orbital altitude, the neutral density around the spacecraft is easily enhanced to this level due to surface outgassing or thruster firings.[12]

We also compared the cases with external magnetic field in the z direction (case S14) and the case with no magnetic field (case S3). However, as long as the neutral density was high, 6.5×10^{18} m^{-3}, there was no significant difference between the two.

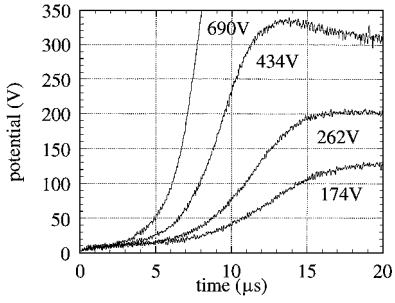

Fig. 14 Temporal variation of potential at $r = 0$ and $z = 175$ cm for different step-bias voltages.

IV. Discussion

In the simulation results, we have seen that the sheath expands explosively from the insulator surface if a sufficient amount of ionization occurs inside the sheath. The sheath boundary expands, however, only up to 50 cm into the z direction and 30 cm into the r direction within 9 μs when the step bias is 434 V. In the arc experiment of Ref. 2, however, we observed that a current path was formed between the arc point on a solar array and the unarced insulator even when they are separated by as much as 270 cm in the face-to-face, z, direction or 140 cm in the side-by-side, r, direction. That the current path is formed indicates that the two points are connected by a field line. Therefore, the jump of the insulator surface potential and the successive ionization near the insulator is not enough to extend the positive sheath from the insulator to the arc point and connect the two points by a field line.

When the current path was formed, that is, two-peak-type discharge in Ref. 2, the arc current showed the increases at time 3–4 μs from arc onset, suggesting that the positive sheath has reached the arc point by that time. Therefore, whether an arc grows by receiving the charge on unarced insulator surface depends on how quickly the positive sheath from the insulator reaches the arc spot before the arc plasma near the solar array loses the conductivity. With ambient electrons alone, the sheath cannot expand as fast and as far, as shown in the computer simulation. Therefore, we need an additional

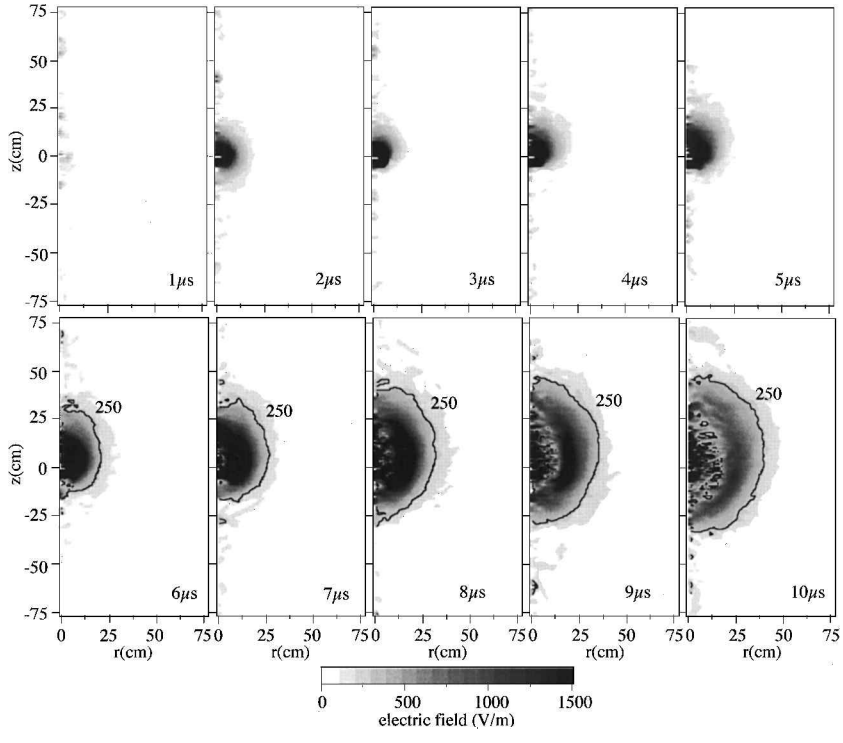

Fig. 15 Time variation of distribution of electric field strength calculated by the computer simulation for case S4.

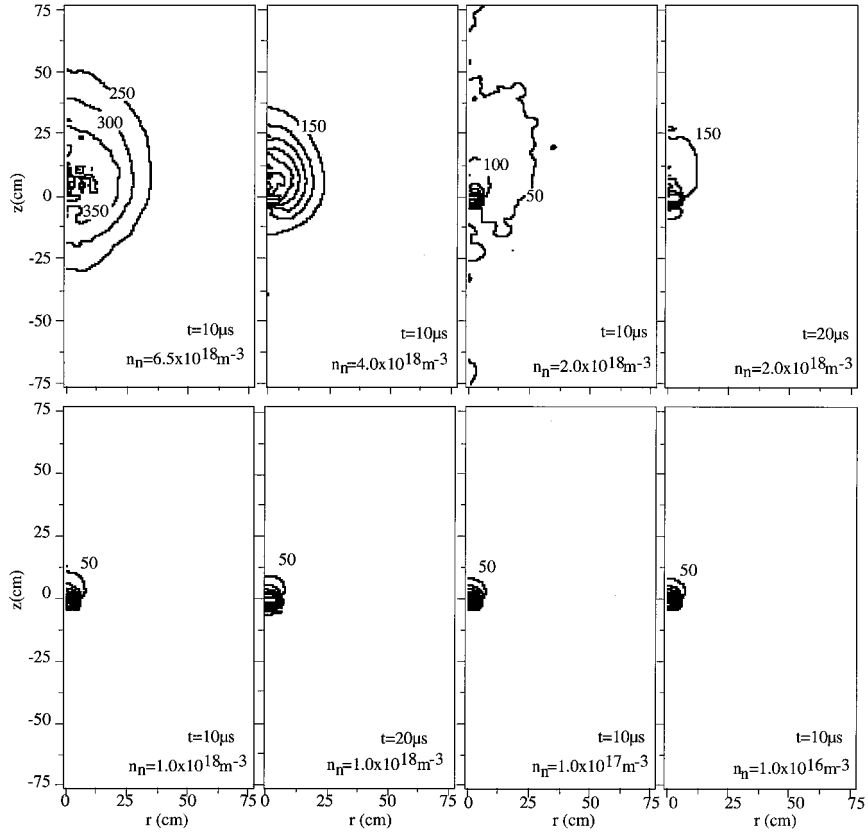

Fig. 16 Spatial distribution of electric potential near insulator at time $t = 10$ or 20 μs calculated for various neutral densities.

mechanism to speed up and extend its expansion. Electrons ejected from the array on arc onset are probably the missing links in the chain, contributing somehow to ionization near the insulator surface. These electrons rapidly diffuse toward the chamber wall. As they diffuse, their negative space charge significantly lowers the space potential around the array and nearby insulators, which has been illustrated as the probe signal V_{pr1} (see Fig. 6 of Ref. 2). If the diffusing electrons find the insulator on their way and accelerate the positive sheath expansion, the current path might be formed between the array and the insulator.

A question now arises on how many of these phenomena observed in the chamber experiment apply to the situation in orbit. In space, there is no chamber wall. Therefore, the plasma potential outside the sheath is not elevated, as we observed both in experiment and simulation. For the case in the chamber, as the plasma potential is elevated, the potential drop inside the sheath decreases, and the expansion speed of the sheath is slowed down. In space, this phenomenon does not occur, and the potential drop across the sheath is maintained and the sheath keeps growing. Therefore, in space, the sheath expansion is faster, which means the current path is formed farther from the arc point. This leads to an unfortunate prediction that the safety distance of 3–4 m derived in the laboratory experiment in Ref. 2 is probably longer for the real situation in space.

Another difference is the gas species. The laboratory experiment and its simulation are carried out with argon as the gas species. In space, if the gas is provided via outgassing from the surface, the major species is water vapor. The sheath expansion is due to the difference of mobility between an ion and an electron, and it scales inversely with the square root of the ionic mass.[9] Therefore, for a pure water vapor, the sheath expansion speed is slower than the case for argon, and the safety distance against the current path formation can be shortened. If the gas is provided via thruster firing, the gas species is determined by the byproduct of the thruster operation. When the gas is heavier than argon, the safety distance must be extended farther.

V. Conclusions

As the size of spacecraft systems and the demand for more power increase, arcing on solar array has become an obstacle against the development of a megawatt-class space platform that generates and delivers its power at a voltage of 400 V or higher. Once an arc occurs on a solar array, the jump in the circuit potential causes the expansion of positive sheath from the unarced insulator that is connected to the arc point through the external circuit. As the positive sheath reaches the arc point, there is an electric field between the array and the insulator. If the conductivity of the plasma is high, the current path is formed between the insulator and the array, feeding energy to the arc plasma. The response of the surrounding plasma to the potential change of the array and insulator surface plays an important role because the arc plasma and the ambient plasma form the current path between the insulator and the arc point. A laboratory experiment and computer simulation have been carried out to study the basic mechanism of positive sheath formation and expansion near the insulator surface.

When a set of simulation parameters that match with the experimental condition as closely as possible was employed, the simulation reproduced the experimentally observed probe signals very well, proving its accuracy. It has shown that the positive sheath expands as a small degree of ionization inside the sheath pushes the sheath boundary outward due to the positive charge of secondary ions. As the sufficient degree of ionization occurs, the sheath expands explosively.

The expansion of the sheath draws a significant amount of electrons from the plasma in the chamber with a finite volume. As the number of electron decreases, the chamber plasma potential outside the sheath is elevated to a positive value of approximately 100 V or higher. This potential increase makes the plasma source located at the chamber end start operating as an electron source, rapidly lowering the plasma potential inside the chamber, yielding the observed peaks of the langmuir probe signal in the experiment.

Although the sheath expansion is extensive when ionization occurs near the insulator surface, its speed and extent are not enough

to explain the current path formation between the remotely located solar array and the insulator surface observed in the experiment. Therefore, it is noted that the contribution of electrons ejected from the arc point at the time of arc onset is probably the key to speed up and to extension of the initial sheath expansion. In future work, we plan to include the motion of electrons ejected from the array in the computer simulation to reveal fully the mechanism of arc development. We also plan to include the plasma source to reproduce the observed peaks of the langmuir probe signal.

Acknowledgments

A part of the computer simulations is carried out with the aid of a research Grant provided by Kyoto University Radio Science Center for Space and Atmosphere. The authors thank K. Aihara of the Institute of Space and Astronautical Sciences and the Kyushu Institute of Technology (KIT) and T. Matsumoto and K. Shiraishi, students of KIT, for their help with the experiment.

References

[1]Hastings, D. E., Cho, M., and Kuninaka, H., "The Arcing Rate for a High Voltage Solar Array: Theory, Experiment and Predictions," *Journal of Spacecraft and Rockets*, Vol. 29, No. 4, 1992, pp. 538–554.

[2]Cho, M., Ramasamy, R., Hikita, M., Tanaka, K., and Sasaki, S., "Plasma Response to Arcing in Ionospheric Plasma Environment: Laboratory Experiment," *Journal of Spacecraft and Rockets*, Vol. 39, No. 3, 2002, pp. 392–399.

[3]Cho, M., Miyata, N., Hikita, M., and Sasaki, S., "Discharge over Spacecraft Insulator Surface in Low Earth Orbit Plasma Environment," *IEEE Transactions on Dielectrics and Electrical Insulation*, Vol. 6, No. 4, 1999, pp. 501–506.

[4]Cho, M., Miyata, N., and Hikita, M., "Effects of Arcing on Insulator Surface Charging Condition in Plasma Environment," AIAA Paper 2000-0872, Jan. 2000.

[5]Birdsall, C. K., and Langdon, A. B., *Plasma Physics via Computer Simulation*, McGraw–Hill, New York, 1981, p. 21.

[6]Cho, M., and Hastings, D. E., "An Analytical and Particle Simulation Study of Localized Semi-Vacuum Gas Breakdown Phenomena on High Voltage Solar Array Surfaces in Low Earth Orbit," *Physics of Fluids B*, Vol. 4, No. 8, 1992, pp. 2614–2625.

[7]Anderson, D. A., Tannehill, J. C., and Pletcher, R. H., *Computational Fluid Mechanics and Heat Transfer*, McGraw–Hill, New York, 1984, p. 250.

[8]Hockney, R. W., and Eastwood, J. W., *Computer Simulation Using Particles*, McGraw–Hill, New York, 1981, p. 215.

[9]Cooke, D. L., and Katz, I., "Ionization-Induced Instability in an Electron Collecting Sheath," *Journal of Spacecraft and Rockets*, Vol. 25, No. 2, 1988, pp. 132–138.

[10]Cho, M., "Ionosphere Ionization Effects on Sheath Structure Around a High-Voltage Spacecraft," *Journal of Spacecraft and Rockets*, Vol. 32, No. 6, 1995, pp. 1018–1026.

[11]Cho, M., "Ionization Around a High-Voltage Body in Magnetized Nonflowing Ionospheric Plasma," *Journal of Spacecraft and Rockets*, Vol. 35, No. 1, 1998, pp. 90–99.

[12]Wulf, E., and von Zahn, U., "The Shuttle Environment: Effects of Thruster Firings on Gas Density and Composition in the Payload Bay," *Journal of Geophysical Research*, Vol. 91, No. A3, 1986, pp. 3270–3278.

A. C. Tribble
Associate Editor